J|A|C|S ARTICLES

Published on Web 09/24/2009

Influence of Amorphous Silica Matrices on the Formation, Structure, and Chemistry of Iron and Iron Oxide Nanoparticles

Dehipalawage Sunil,[†] Jinquan Dong,[‡] and Harry D. Gafney*,[‡]

Department of Physics, Queensborough Community College, City University of New York, Bayside, New York 11364, and Department of Chemistry, Queens College, City University of New York, Flushing, New York 11367

Received April 23, 2009; E-mail: harry.gafney@qc.cuny.edu

Abstract: $Fe(CO)_5$ physisorbs onto Corning's code 7930 porous Vycor glass (PVG) and dried ($\leq$200 °C), base-catalyzed (NH_3) tetramethoxysilane/methanol/water xerogels. Although chemically and structurally similar matrices, 488-nm photolysis of the physisorbed complex yields ca. equal amounts of Fe^0 and Fe_2O_3 in PVG, but only Fe_2O_3 in the xerogel. Mossbauer, EXAFS, and XANES results give no indication the photoproducts bind to either silica matrix, and consolidation of the PVG matrix leads to $Fe^0-Fe_2O_3$ nanoparticle formation with little change in the Fe^0/Fe(III) ratio. PVG serves as a template defining the particle diameter and interparticle spacing, whereas consolidation of the xerogel does not result in nanoparticle formation. Instead, ca. 20% of the octahedrally coordinated Fe(III) converts to tetrahedral coordination during consolidation. The photoproducts within these porous silica matrices reflect a competition between aggregation and oxidation, where the extent and most likely the rate of aggregation are functions of the correlation lengths of these amorphous matrices. With a correlation length of 22 ± 1 nm, aggregation exceeds oxidation in PVG and limits oxidation to the outer periphery, thereby creating particles whose Fe^0/Fe(III) ratio is unaffected by air or water released during consolidation of the silica matrix. The correlation length of the xerogel, $\leq$1 nm, limits aggregation of the primary photoproduct and favors smaller particles. As a result, the primary photoproducts in the xerogel do not achieve sufficient size to limit oxidation to the outer periphery of the particle, and the primary photoproduct oxidizes, forming only Fe_2O_3. Desorption of decomposition products derived from the xerogel precursors creates a dynamic surface that limits nanoparticle growth during annealing. Desorption also disrupts the growing silicate matrix, creating sites that facilitate the change from octahedrally to tetrahedrally coordinated Fe(III) in the xerogel.

Introduction

With properties differing from those of their molecular and bulk forms, considerable research effort focuses on the synthesis and properties of nanosized materials. Accessing the nanometer domain usually requires an external reagent or medium that controls, or in some manner limits, particle growth.[1] Mixtures of tri-*n*-octylphosphine oxide (TOPO) and tri-*n*-octylphosphine (TOP), for example, produce a narrow size distribution of monodispersed, crystalline II−IV quantum dots from organometallic precursors.[2,3] Identification and characterization of the role of hexylphosphonic acid, HPA, an impurity in TOPO, broadened the number of reagents capable of serving as precursors and the number of solvents that yield not only a narrow size distribution of crystalline CdSe quantum dots, but shapes with differing aspect ratios.[4−6]

In addition to surfactants, colloids,[7] metal and metal oxide surfaces,[8] sol−gels,[9] carbon nanotubes,[10] DNA,[11] SiO_2 films,[12] silica areo- and xerogels,[13] and porous silica glasses[14] also serve as scaffolds that limit particle growth and yield narrow distributions of nanometer diameter particles. In most cases, however, the mechanisms by which these media influence particle growth and/or limit aggregation are not known. The narrow distributions of particle sizes achieved in sol−gels, xerogels, and porous glasses are particularly surprising since these are amorphous materials characterized by little structural order.[15] These materials vary from sample to sample and possess structural variations within the same sample. Furthermore, the structural variations are thought to produce variations in the distributions of surface silanol functionalities from one position to another within the

[†] Queensborough Community College.
[‡] Queens College.

(1) Qu, L.; Peng, Z. A.; Peng, X. *Nano Lett.* **2001**, *1*, 333–337.
(2) Peng, Z. A.; Peng, X. *J. Am. Chem. Soc.* **2001**, *123*, 168.
(3) Rafeletos, G.; Norager, S.; O'Brien, P. *J. Mater. Chem.* **2001**, *11*, 2542–2544.
(4) Peng, Z. A.; Peng, X. *J. Am. Chem. Soc.* **2001**, *123*, 1389.
(5) Peng, X. *Chem.—Eur. J.* **2002**, *8*, 334–339.
(6) Peng, X.; Yu, W. W. *Angew. Chem., Int. Ed.* **2002**, *41*, 2368.
(7) (a) Compton, O. C.; Osterloh, F. E. *J. Am. Chem. Soc.* **2007**, *129*, 7793. (b) Chen, C.-C.; Hsu, C.-H.; Kuo, P.-L. *Langmuir* **2007**, *23*, 6801. (c) Lee, B. H.; Kwon, K.-W.; Shim, M. *J. Mater. Chem.* **2007**, *17* (13), 1284. (d) Murthy, V. S.; Rana, R. K.; Wong, M. S. *J. Phys. Chem. B* **2006**, *110*, 25619. (e) Shukla, D.; Mehra, A. *Langmuir* **2006**, *22*, 9500. (f) Rhodes, S. K.; Lewis, J. A. *J. Am. Ceram. Soc.* **2006**, *89*, 1840. (g) Jiang, Z.-J.; Liu, C.-Y.; Liu, Y. *Appl. Surf. Sci.* **2004**, *233*, 135.
(8) (a) Yoshinaga, M.; Takahashi, H.; Yamamoto, K.; Muramatsu, A.; Morikawa, T. J. *Colloid Interface Sci.* **2007**, *309*, 149. (b) Jones, P. M.; Dunn, S. *Nanotechnology* **2007**, *18*, 185702. (c) Wang, Y.; Luo, Z.; Li, B.; Ho, P. S.; Yao, Z.; Shi, L.; Bryan, E. N.; Nemanich, R. J. *J. Appl. Phys.* **2007**, *101* (12), 124310. (d) Henley, S. J.; Carey, J. D.; Silva, S. R. P. *Phys. Rev. B* **2005**, *72* (19), 195408. (e) Berdunov, N.; Mariotto, G.; Balakrishnan, K.; Murphy, S.; Shvets, I. V. *Surf. Sci.* **2006**, *600* (21), L287.

10.1021/ja9031874 CCC: $40.75

same sample and from sample to sample,[15] yet these amorphous materials yield narrow distributions of particle sizes comparable to those obtained in other media.[14]

Our interest in particle growth and size in amorphous silicas stems from the photocatalytic and optical applications of metal and/or metal oxide particles generated in these matrices. With a catalyst derived from an organometallic precursor, particularly monometallic precursors adsorbed onto a support, a reoccurring question is whether aggregation or size is required for catalytic activity. In the photocatalyzed conversion of CO_2 to CH_4, formally an eight-electron process, by tungsten oxides adsorbed onto porous Vycor glass, for example, shifts in the electronic spectrum suggest aggregation, yet the catalytic reaction occurs prior to these spectral changes, and the spectral changes are not accompanied by measurable changes in photocatalytic efficiency.[16] In optical applications, photodeposition of nanometer diameter metal and/or metal oxide particles in porous silicas followed by thermal consolidation to a nonporous glass produces refractive index patterns that guide, focus, and diffract light.[17] However, the factors that control the optical performance of the structures are not well understood. Parameters dependent on pattern resolution, such as light dispersion, improve as a result of the 30−40% reduction in sample volume that accompanies matrix consolidation.[18] Structures created by the photodeposition of transition metals and their oxides, however, often lose transparency and transmissivity as a result of matrix consolidation. The electronic absorptions shift to longer wavelength with no measurable change in dopant composition. Originally attributed to increases in particle size, subsequent experiments show that, while size influences the spectroscopy, other as yet unidentified factors must also play a significant role.[17]

To gain insights into how porous silica matrices influence photodeposited transition-metal and metal oxide nanoparticles, one avenue of investigation in this laboratory focuses on identifying structural and/or chemical factors of nanoporous, amorphous silica matrices that influence the chemistry, aggregation, size, and distribution of metal−metal oxide nanoparticles within the matrices. Ascertaining the role of an amophorous matrix, however, is challenging since, by its very nature, an amorphous matrix possesses no structural order. In reality, an amorphous matrix is characterized by differing length scales of structural and chemical order which, as noted, varies within the same sample and from sample to sample. The approach that has evolved in this laboratory centers on comparisons of the chemistry and aggregation of a probe molecule in Corning's code 7930 porous Vycor glass (PVG)[15] and dried (≤200 °C), base-catalyzed (NH_3) tetramethoxysilane/methanol/water (TMOS/MeOH/H_2O) xerogels.[17]

PVG and dried (≤200 °C) TMOS/MeOH/H_2O xerogels are nodular materials with a randomly dispersed pore structure throughout both matrices.[17] Interior and exterior surfaces of both materials possess individual and associated or hydrogen-bonded silanol groups dispersed on the silica surface, and thermal consolidation of both materials yields consolidated, nonporous SiO_2 glasses.[15,17] Although chemically and structurally similar, these are fundamentally different materials. Heated above its sintering temperature, 1105 ± 18 °C,[14b,15] PVG is an acid-leached, porous glass,[15] whereas the dried (≤200 °C) TMOS/MeOH/H_2O xerogel is a partially polymerized silica.[17] The experiments described here exploit these similarities and differences to explore the role of these amorphous matrices in the chemistry of the photoproducts derived from $Fe(CO)_5$ and their aggregation within the matrices.

$Fe(CO)_5$ physisorbs into both matrices without a change or significant distortion of its primary coordination shell.[14b] A 488-nm photolysis of the adsorbed complex, designated $Fe(CO)_5$(ads), in air leads to rapid decarbonylation, producing ca. equal amounts of elemental iron, Fe^0, and Fe_2O_3 in PVG,[19] but only Fe_2O_3 in the dried xerogel.[20] Water is ubiquitous in

(9) (a) Moncada, E.; Quijada, R.; Retuert, J. *Nanotechnology* **2007**, *18*, 335606. (b) Faheem, Y.; Joya, K. S. *Appl. Phys. Lett.* **2007**, *91*, 063115. (c) Carta, D.; Mountjoy, G.; Navarra, G.; Casula, M. F.; Loche, D.; Marras, S.; Corrias, A. *J. Phys. Chem. C* **2007**, *111*, 6308. (d) Boev, V. I.; Soloviev, A.; Rodriguez-Gonzalez, B.; Silva, C. J. R.; Gomes, M. J. M. *Mater. Lett.* **2006**, *60*, 3793–3796. (e) Encheva, G.; Samuneva, B.; Djambaski, P.; Kashchieva, E.; Paneva, D.; Mitov, I. *J. Non-Cryst. Solids* **2004**, *345*, 615–619. (f) Sugimoto, T.; Zhou, X.; Muramatsu, A. *J. Colloid Interface Sci.* **2003**, *259* (1), 43–52. Cheung, S. H.; Dave, B. C. *Mater. Res. Soc. Symp. Proc. (Org./Inorg. Hybrid Mater.)* **2002**, *726*, 173–177.

(10) (a) Bale, S.; Asuri, P.; Karajanagi, S. S.; Dordick, J. S.; Kane, R. S. *Adv. Mater.* **2007**, *19*, 3167–3170. (b) Ou, Y.-Y.; Huang, M. H. *J. Phys. Chem. B* **2006**, *110*, 2031–2036. (c) Sun, C.-L.; Chen, L.-C.; Su, M.-C.; Hong, L.-S.; Chyan, O.; Hsu, C.-Y.; Chen, K.-H.; Chang, T.-F.; Chang, L. *Chem. Mater.* **2005**, *17*, 3749–3753. (d) Guo, D.-J.; Li, H.-L. *J. Electroanal. Chem.* **2004**, *573*, 197–202.

(11) (a) Park, S. Y.; Lytton-Jean, A. K. R.; Lee, B.; Weigand, S.; Schatz, G. C.; Mirkin, C. A. *Nature (London)* **2008**, *451*, 553–556. (b) Buckman, J.; Sengupta, B.; Ritchie, C. M.; Petty, J. T. The Role of Base Specific Interactions in the Formation Silver Nanoclusters. *Abstracts*, 59th Southeast Regional Meeting of the American Chemical Society; American Chemical Society: Washington, DC, 2007; GEN-614. (c) Samson, J.; Drain, C. M.; Varotto, A. Plasmid DNA as a Template for Metal Nanoparticle Formation. *Abstracts*, 234th ACS National Meeting; American Chemical Society: Washington, DC, 2007; COLL-185. Shang, L.; Wang, Y.; Huang, L.; Dong, S. *Langmuir* **2007**, *23*, 7738–7744. (d) Noyong, M.; Gloddek, K.; Mayer, J.; Weirich, Th.; Simon, U. *J. Cluster Sci.* **2007**, *18*, 193–204. (e) Srivastava, S.; Samanta, B.; Arumugam, P.; Han, G.; Rotello, V. M. *J. Mater. Chem.* **2007**, *17*, 52–55. (f) Kim, H. J.; Roh, Y.; Hong, B. *J. Vacuum. Sci. Technol., A* **2006**, *24*, 1327–1331. (g) Lou, X.; Wang, C.; He, L. *Biomacromolecules* **2007**, *8*, 1385–1390.

(12) (a) Arai, N.; Tsuji, H.; Adachi, K.; Kotaki, H.; Gotoh, Y.; Ishikawa, J. *Jpn. J. Appl. Phys., Part 1* **2007**, *46*, 6260–6266. (b) de la Pena O'Shea, V. A.; Alvarez-Galvan, M. C.; Campos-Martin, J. M.; Menendez, N. N.; Tornero, J. D.; Fierro, J. L. G. *J. Inorg. Chem.* **2006**, *24*, 5057–5068. (c) Pal, B. N.; Chakravorty, D. *J. Phys. Chem. B* **2006**, *110*, 20917–20921. (d) Heng, C. L.; Finstad, T. G.; Li, Y. J.; Gunnaes, A. E.; Olsen, A.; Storas, P. *Microelectron. J.* **2005**, *36*, 531–535. (e) Pal, B. N.; Chakravorty, D. *J. Phys. Chem. B* **2006**, *110*, 20917–21.

(13) (a) Carta, D.; Mountjoy, G.; Navarra, G.; Casula, M. F.; Loche, D.; Marras, S.; Corrias, A. *J. Phys. Chem. C* **2007**, *111*, 6308–6317. (b) Tai, Y.; Watanabe, M.; Murakami, J.; Tajiri, K. *J. Mater. Sci.* **2007**, *42*, 1285–1292. (c) Zhang, D.-Q.; Wang, S.-J.; Sun, H.-S.; Wang, X.-L.; Cao, M.-S. *J. Sol-Gel Sci. Technol.* **2007**, *41*, 157–161. (d) Moore, J. G.; Lochner, E. J.; S., A. E. *Angew. Chem.* **2007**, *46*, 8653–8655.

(14) (a) Murase, N.; Yazawa, T. *J. Am. Ceram. Soc.* **2001**, *84*, 2269–2273. (b) Gafney, H. D.; Sunil, D.; Devi, P. S.; Dong, J.; McQuade, A. W; Mendoza, E. A. *Comments Inorg. Chem.* **2003**, *24* (3−4), 69–136.

(15) (a) Iler, R. K. *The Chemistry of Silica*; Wiley-Interscience: New York, 1979; p 3. (b) Scholz, H. *Glass: Nature, Structure and Properties*; Springer: New York, 1991. (c) Enke, D.; Janowski, F.; Schwieger, W. *Microporour Mesoporous Mater.* **2003**, *60*, 19–30. Janowski, V. F.; Heyer, W. *Z. Chem.* **1989**, *19*, 1. Janowski, F.; Enke, D. *Handb. Porous Solids* **2002**, *3*, 1432–1542. (d) Enke, D.; Janowski, F.; Gille, W.; Schwieger, W. *Colloids Surf., A* **2001**, *187*, 131–139.

(16) (a) Gafney, H. D.; Simon, R. C.; Mendoza, E. *Inorg. Chem.* **1988**, *27*, 2733. (b) Gafney, H. D.; Xu, S.-P. *Proc. Electrochem. Soc.* **1993**, *93*, 38.

(17) Brinker, J. C.; Scherer, G. W. *Sol-Gel Science The Physics and Chemistry of Sol-Gel Processing*; Academic Press: New York, 1989; Vol. 471, pp 515−610.

(18) (a) Gafney, H. D.; McQuade, A. W.; Sunil, D. *Proc. SPIE* **1999**, *3778*, 139. (b) Gafney, H. D.; McQuade, A. W.; Sunil, D. *Appl. Spectrosc.* **2000**, *54* (6), 869.

(19) Gafney, H. D.; Sunil, D.; Rafailovich, M.; Sokolov, J. *Inorg. Chem.* **1993**, *32*, 4489.

(20) Gafney, H. D.; Mendoza, E. A.; Wolkow, E.; Sunil, D; Sokolov, J.; Rafailovich, M. H. *Langmuir* **1991**, *7*, 3046.

these matrices, and the difference in the photoproducts formed was originally attributed to differences in the water contents of the two matrices.[20] However, data presented here show that the total amount of water evolved during consolidation of both matrices exceeds the amount of $Fe(CO)_5$ initially adsorbed, and more extensive drying fails to change the photoproduct distribution. Consolidation of the PVG matrix increases the $Fe^0-Fe_2O_3$ particle diameter to 10 ± 1 nm with a $\leq 12\%$ change in the Fe^0/Fe(III) ratio, while consolidation of the xerogel under equivalent conditions does not result in particle growth. Instead, ca. 20% of the iron initially present as octahedrally coordinated Fe(III) changes to tetrahedrally coordinated Fe(III). Water is most likely the oxidant, but water content is not the sole determinant of photoproduct chemistry. Rather, differences in the photoproducts in the two matrices reflect a competition between aggregation and oxidation. Differences in the rates and extents of aggregation within the two matrices are consequences of fundamental, short-range, structural differences not evident in the topologies of silica surfaces. Both amorphous matrices consolidate to nonporous silica glasses, but the dynamics of consolidation of the two matrices differentiate not only surface diffusion and ultimately particle size, but the chemistry of the adsorbates on these silica surfaces.

Experimental Section

Materials. $Fe(CO)_5$ (Aldrich) was used without further purification since the electronic and IR spectra of the vapor were in excellent agreement with published spectra.[21] Tetramethylorthosilicate, TMOS (Aldrich) and methanol (Aldrich) were used as received. Xerogels were prepared by previously described procedures with gelation catalyzed by the addition of two drops of 10^{-3} M NH_3.[20,22,23] After addition of NH_3, the sols were poured into glass or stainless steel containers or Teflon molds to create xerogels of the desired size and shape. The containers and molds were covered with a polyethylene film to minimize evaporation and allowed to gel at room temperature. After 48 h, the polyethylene film was punctured with a pin to enhance alcohol and water evaporation. An additional hole was punched in the polyethylene each day for the next two to four weeks. The resulting xerogels, which were generally cast in the form of 12×25 mm^2 rectangles with a thickness of 0.5−1.0 mm, were then placed in a vacuum desiccator and dried for 24 h under reduced pressure ($p \leq 10^{-2}$ Torr) at room temperature. After being dried under reduced pressure, the samples were placed in a programmable furnace (Thermolyne model F46128CM-75), heated to 200 °C at a rate of 0.5 °C/min, maintained at 200 °C for at least 24 h, and then cooled to room temperature at a rate of 2 °C/min. The cooled xerogels were stored in a vacuum desiccator at room temperature under reduced pressure.

Polished 25 mm × 25 mm × 2 mm thick pieces of Corning's code 7930 porous Vycor glass were continuously extracted with distilled water for at least 24 h and then dried at room temperature under vacuum ($p \leq 10^{-2}$ Torr). The dried samples were calcined at 550 °C for at least 24 h and stored at 550 °C until needed. At that point, the sample was removed from the oven, placed in a vacuum desiccator, and allowed to cool to room temperature.

Impregnation Procedures. $Fe(CO)_5$ impregnation of the dried xerogels and PVG samples was by previously described vapor deposition techniques.[21] The number of moles of complex adsorbed per gram of the xerogel was determined by comparing the absorbance of the doped sample at 350 nm to a previously determined calibration plot developed for PVG.[21] On the basis of this method, the samples examined in these experiments contain either 10^{-6} or 10^{-4} mol of $Fe(CO)_5$/g of PVG or the xerogel. Differences in the xerogel thickness and the flatness of the xerogel samples relative to each other and to the PVG samples, however, introduce an uncertainty in the calculated loading of the xerogel samples. As a result, the reported loadings of the xerogel samples are more useful in a relative, rather than absolute, sense.

Photolysis Procedures. The impregnated samples were irradiated in air with 488-nm light from a Coherent Innova Ar^+ laser. The laser beam was expanded to completely expose the front surface of the sample, and the average incident intensity, typically 1.1×10^{-6} einstein/(s cm^2), was measured with a Coherent model 210 power meter.

Physical Measurements. UV−vis spectra were recorded on an Aviv model 14S spectrophotometer relative to that of untreated PVG or xerogel. Room and low-temperature (20 K) Mossbauer spectra were recorded with a previously described spectrometer equipped with a 10 mC ^{57}Fe source (^{57}Co/Rh).[20] The spectrometer was calibrated with a 25 μm thick α-Fe standard (Amersham, ≥99%), and all data were fit with Lorenzian functions using the χ^2 test to determine the quality of the fit. Fluorescent iron EXAFS and XANES spectra were recorded on the X-10C beamline of the National Synchrotron Light Source at Brookhaven National Laboratory. Absorption edges were normalized by fitting polynomials to the pre-edge region, extrapolating the fit over the entire EXAFS range, and subtracting it point by point from the data. Corrections for background absorption were by a previously described procedure.[24]

Scanning electron micrographs were recorded on a Hitachi model S570 scanning electron microscope, while transmission electron micrographs were recorded on a Jeol 100CX transmission electron microscope operating in the bright-field mode with an electron beam energy of 100 keV. All samples were dried extensively, coated with gold, and examined according to previously described procedures.[25] The surface morphology of the samples was examined with a Digital Instruments Nanoprobe IIIa atomic force microscope. Pieces (0.5 mm × 0.5 mm) of PVG or the dried xerogel were mounted onto metal disks and imaged in the tapping mode with the cantilever oscillating at or near the resonance frequency with an amplitude typically ranging from 20 to 100 nm. Horizontal and vertical deviations were calibrated with a metal grid standard. The surface roughness, the deviation from a hypothetical plane defined by the median of the cantilever tip oscillation, was calculated with the supplied software.

Results

Corning's code 7930 PVG derives from a 96% SiO_2, 3% B_2O_3, and 1% Na_2O and Al_2O_3 melt. The borate phase separates on cooling, and acid leaching of that phase yields a transparent (50% T at 259 nm vs air), porous glass composed of 3−5 μm diameter silica nodules with the spaces between the nodules defining an interconnected porosity randomly dispersed throughout the material.[26] Higher resolution measurements reveal the 3−5 μm diameter nodules are themselves aggregates of smaller,

(21) Gafney, H. D.; Darsillo, M. S.; Paquette, M. *J. Am. Chem. Soc.* **1987**, *109*, 3275.
(22) Dong, J. Fabrication and Characterization of Porous Glass Derived Optical Materials and Devices. Ph.D. Thesis, City University of New York, 1997; pp 43−44.
(23) Zarsycky, J. In *Ultrastructure Processing of Ceramics, Glasses, and Composites*; Hench, L. L., Ulrich, D. R., Eds.; Wiley: New York, 1984; p 43.
(24) Gafney, H. D.; Mendoza, E. A.; Wolkow, E.; Sunil, D.; Rafailovich, M.; Sokolov, J.; Long, G.; Jemian, P. *Appl. Phys. Lett.* **1990**, *57* (3), 209.
(25) Gafney, H. D.; Sunil, D.; Rafailovich, M. H.; Sokolov, J.; Gambino, R. J.; Halada, G.; Huang, D. M. *J. Non-Cryst. Solids* **2003**, *319*, 154–162.
(26) (a) Kim, M.-H.; Glinka, C. J. *Microporous Mesoporous Mater.* **2006**, *91* (1−3), 305–311. (b) Levitz, P.; Ehret, G.; Sinha, S. K.; Drake, J. M. *J. Chem. Phys.* **1991**, *95* (8), 6151–61. (c) Wiltzius, P.; Bates, F. S.; Dierker, S. B.; Wignall, G. D. *Phys. Rev. A* **1987**, *36* (6), 2991–4. (d) Ito, Y.; Yamashina, T.; Nagasaka, M. *Appl. Phys. (Berlin)* **1975**, *6* (3), 323–6.

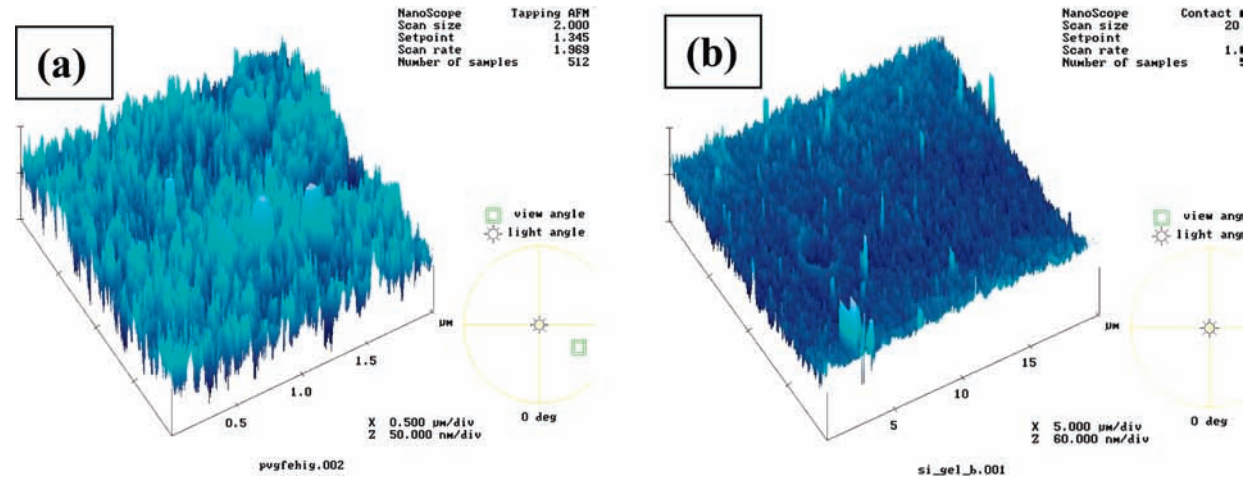

Figure 1. AFM images of the surfaces of (a) PVG and (b) dried TMOS/MeOH/H_2O xerogel. The z axes in both images are 50 nm/division.

300−600 nm diameter SiO_2 nodules with the surfaces of these nodules covered by sharp stalagmite-like features (Figure 1a). The peaks along the edges of eight different PVG samples yield an average height of 40 ± 20 nm with an average width of 40 ± 20 nm. The surface is characterized by an irregularity, i.e., a deviation from a hypothetical flat plane, of ±440 nm. N_2 adsorption−desorption measurements yield an isotherm similar to that previously reported (IUPAC classification type H2) with relatively little adsorption at low pressure followed by a sharp increase in N_2 adsorption at higher pressure.[27] Considerable hysteresis occurs between adsorption and desorption at higher pressures. The surface area calculated from the N_2 adsorption isotherm, 184 ± 10 m^2/g of PVG, is within experimental error of previous measurements, while desorption isotherms yield a narrow range of pore diameters, 10 ± 1 nm, which are within experimental error of reported pore diameters.[28]

Base-catalyzed (NH_3) gelation of a TMOS/MeOH/H_2O solution at room temperature followed by slow drying at room temperature under reduced pressure and then at 200 °C produces a transparent (50% T at 390 nm vs air), porous, glasslike material. AFM imaging reveals a structural motif similar to that of PVG with 5−8 μm diameter silica nodules and the intervening spaces defining a porosity randomly distributed throughout the material. As in PVG, higher resolution measurements show the 5−8 μm diameter nodules are aggregates of 70−200 nm diameter SiO_2 nodules. At these levels of resolution, the only apparent difference between PVG and the dried xerogel is the nodules visible in PVG appear more spherical whereas those in the xerogel are more irregular in shape. Stalagmite-like features are also present on the surfaces of the smaller nodules in the xerogel (Figure 1b), but the number and size are smaller than those on PVG. The features evident along the edges of the images of four different xerogel samples range from 5 to 20 nm wide and from 10 to 20 nm high. The xerogel surfaces are characterized by an irregularity of ±286 nm. The shape of the N_2 adsorption−desorption isotherms obtained with the xerogels is similar to that previously reported (IUPAC classification type H1) for xerogels prepared in a similar manner.[27] These differ from those obtained with PVG with relatively little hystersis between adsorption and desorption and the largest amount of N_2 adsorbed at relatively low pressure. The surface area calculated from the adsorption isotherm is 508 ± 18 m^2/g, which is slightly smaller than previous determinations, while the desorption isotherm yields a range of pore diameters ranging from 0.5 nm to 1−2 μm.

Water is ubiquitous in both materials, and its desorption occurs over a wide temperature range. The first significant weight losses in the 80−150 °C range are followed by a continued decline in sample weight, although at a reduced rate. A marked increased in weight loss occurs at ca. 500 °C in the xerogel and 600 °C in PVG. Diffuse reflectance FTIR (DRIFT) confirms that the initial weight losses are due to the desorption of physisorbed water from PVG, and physisorbed water and methanol from the xerogels. The losses at the higher temperature reflect the loss of water derived from the silanol condensation to form a consolidated glass.

In PVG dried at 500 °C for 24 h, the free silanols exhibit a sharp band at 3755 cm^{-1} with a distinct, lower intensity shoulder at 3650 cm^{-1} assigned to the associated or hydrogen-bonded silanols.[14b,21,22] TMOS/MeOH/H_2O xerogels dried at 200 °C exhibit a free silanol band at 3744 cm^{-1} with the associated silanols appearing as a shoulder at 3650 cm^{-1} along with bands at 2959 and 2852 cm^{-1} due to OCH_3 functionalities within the xerogel.[14b,20,22] Normalizing both spectra to the intensity of the free silanol band and subtracting one from the other shows that the relative intensities of the 3650 cm^{-1} band are similar, suggesting that the ratio of free to associated silanols is not that different in the two matrices. The xerogel, however, exhibits a slightly stronger, broad absorption centered at 3450 cm^{-1}, implying that the xerogel possesses a higher content of chemisorbed water.[20]

Thermomechanical analyses (TMA) reveal slight contractions accompany the loss of physisorbed water from both matrices at 100 °C, but the contractions are not sufficient to change the surface area of either matrix. The surface area of PVG changes little up to 600 °C and then declines smoothly with the steepest decline in the 900−1000 °C region (Figure 2). Above 600 °C, the individual silica nodules broaden and meld together with an accompanying decline in the silanol bands at 3755 and 3650 cm^{-1}. The surface area of the xerogel, 508 ± 18 m^2/g at room temperature, changes little up to 300 °C, but then begins to oscillate, showing both increases and decreases in surface area in the 300−500 °C range followed by a decline in the 500−800 °C range (Figure 2). Each of four xerogel samples examined exhibit oscillations in surface area in the 300−500 °C range

(27) Reference 22, pp 74 and 85.
(28) Thommes, M.; Smarsly, B.; Groenewolt, M.; Ravikovitch, P. I.; Neimark, A. V. *Langmuir* **2006**, *22* (2), 756–764.

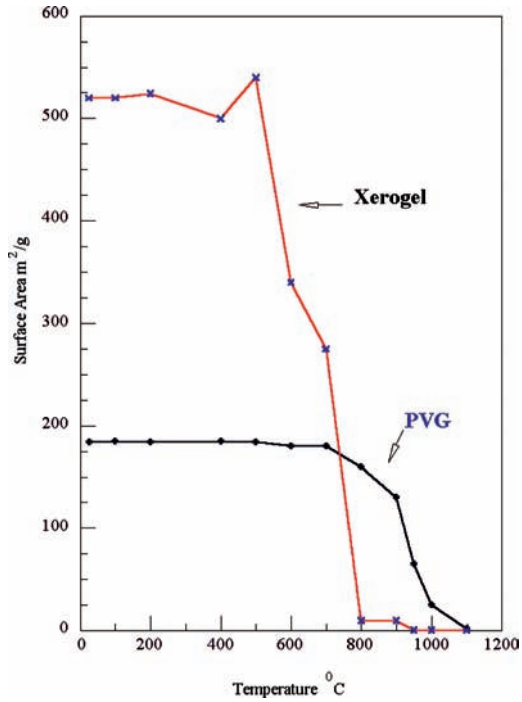

Figure 2. Surface area of PVG and dried TMOS/MeOH/H_2O xerogel as a function of temperature.

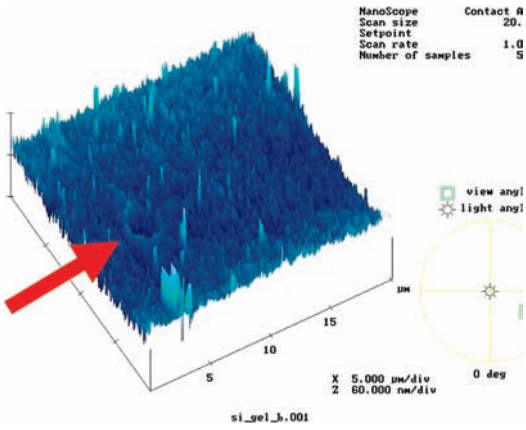

Figure 3. Crater (arrow) formed by the desorption of gaseous decomposition products during heating of TMOS/MeOH/H_2O xerogel.

with no apparent pattern to the oscillations. Differential scanning calorimetry (DSC) reveals two exothermic processes in this temperature range. One occurs at 380 °C and is accompanied by a decline in the intensity of the Si−OCH_3 bands at 2959 and 2852 cm^{-1} and the appearance of a slight gray or gray-black color in the xerogel. The other occurs at 440 °C and is accompanied by a loss of the gray or gray-black color. AFM imaging of xerogels shows that these exothermic processes lead to the formation of many sharp-edged craters (Figure 3) on the xerogel surface. Beyond this chaotic domain, which is not present in the consolidation of PVG (Figure 2), the consolidation of the xerogel parallels that of PVG, but at slightly lower temperatures. Like those of PVG, SEM images of xerogels heated to 600 °C show the silica nodules broadening and melding together with a corresponding decline in the intensity of the 3744 cm^{-1} silanol band. The glass transition temperature of PVG, determined by extrapolating onsets,[29] 848 ± 20 °C,[22] is similar to that reported by Scholz, 910 °C.[30] Subtracting two DTA scans on the same PVG sample reveals an exothermic process at 1105 ± 18 °C that is attributed to the release of surface energy due to viscous sintering. An exothermic process at 1120 °C is also attributed to the viscous sintering of the SiO_2 glass derived from the consolidated xerogel.

$Fe(CO)_5$ physisorbs onto PVG without degradation,[21] whereas adsorption of 10^{-4} mol of $Fe(CO)_5$/g onto a freshly prepared TMOS/MeOH/H_2O xerogel results in immediate decomposition of ≥98% of the complex within the time of adsorption. Drying the xerogel at 35 °C under reduced pressure, $\leq 10^{-2}$ Torr, and then at 85 °C for at least 24 h prior to adsorption reduces the amount of decomposition occurring. Mossbauer spectra of $Fe(CO)_5$ adsorbed onto the dried xerogel exhibit a doublet with an isomer shift of −0.087 mm/s and a quadrupole splitting of 2.57 mm/s, which are within experimental error of those of $Fe(CO)_5$ physisorbed onto PVG and neat $Fe(CO)_5$.[20] The absence of detectable decomposition products in the dried xerogel indicates that drying the xerogel prior to adsorption reduces $Fe(CO)_5$ decomposition to ≤10% of the adsorbed complex.

A 488-nm photolysis of the complex on the dried silica supports leads to rapid CO evolution. With the same excitation intensity, the rates of $Fe(CO)_5$ decomposition on the xerogel are within experimental error of those on PVG, implying the quantum efficiency of decomposition on the xerogel is equivalent to that on PVG, $\Phi_{dec} = 0.96 \pm 0.05$.[21] However, XANES, EXAFS, and Mossbauer spectra of photoproducts formed in the xerogel differ from those in PVG. In PVG, Mossbauer doublets at 0.13 ± 0.01 mm/s with a quadrupole splitting of 0.57 ± 0.01 mm/s and at 0.52 ± 0.05 mm/s with a quadrupole splitting of 0.64 ± 0.06 mm/s indicate octahedrally coordinated Fe^{3+} and elemental iron, Fe^0.[31] EXAFS and XANES confirm both forms of iron in the samples, and the relative intensities of the Mossbauer spectra yield 42 ± 12% as the Fe^0/ Fe(III) ratio in the PVG samples examined. Mossbauer spectra of the photoproduct generated in the xerogel (Figure 4a), however, consist of a single doublet with an isomer shift of 0.40 ± 0.01 mm/s and a quadrupole splitting of 0.95 ± 0.01 mm/s. Although not identical to those found in PVG, in both matrices, the isomer shifts and quadrupole splittings fall within the range of values reported for octahedrally coordinated Fe(III).[19,20,31] The major difference is the absence of any evidence of elemental iron formation in the xerogel. In fact, no set of experimental conditions examined to date leads to elemental iron in the xerogel. Varying the initial $Fe(CO)_5$ loading from 10^{-6} to 10^{-4} mol/g, carrying out the photolysis in the presence and absence of air, changing the excitation wavelength from 488 to 350 nm, or more extensive drying of the xerogel (one month at 200 °C) prior to $Fe(CO)_5$ impregnation fails to produce elemental iron in the xerogel.

EXAFS and XANES spectra of TMOS/MeOH/H_2O xerogel samples impregnated with 10^{-4} mol/g $Fe(CO)_5$ and photolyzed with 488-nm light in air (Figure 5) corroborate the Mossbauer spectra. Normalized to the intensity of the first oscillation of the EXAFS absorption at 7150 eV, which is proportional to the total iron content, the intensity of the XANES pre-edge feature at 7113 eV (Figure 5) is equivalent to the normalized

(29) Takamori, T.; Tomozawa, M. *J. Am. Ceram. Soc.* **1978**, *61* (11−12), 509.
(30) Scholze, H. *Glass: Nature, Structure and Propertries*; Springer-Verlag: New York, 1991; p 192.
(31) (a) Gafney, H. D.; Sunil, D.; Rafailovich, M.; Sokolov, J. *Inorg. Chem.* **1993**, *32*, 4489.

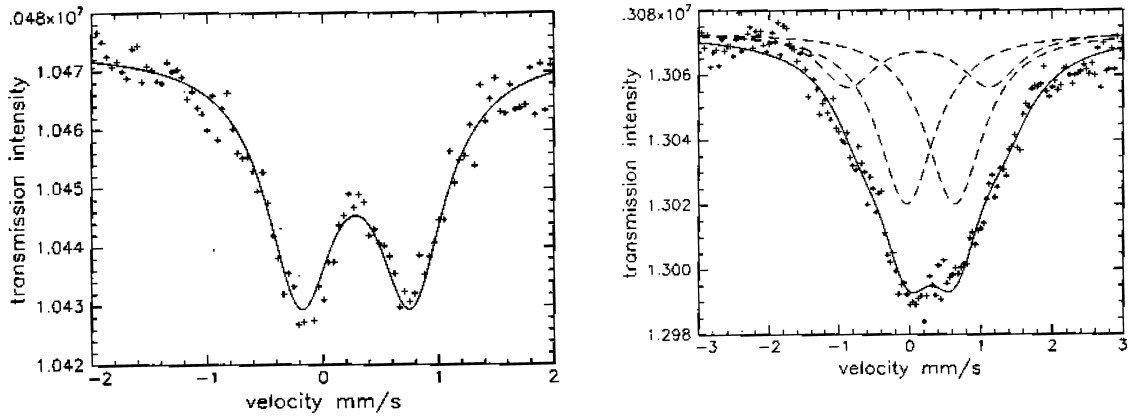

Figure 4. Mossbauer spectrum of (a) the photoproduct generated in TMOS/MeOH/H_2O xerogel and (b) the photoproduct after consolidation of the xerogel matrix at 1200 °C .

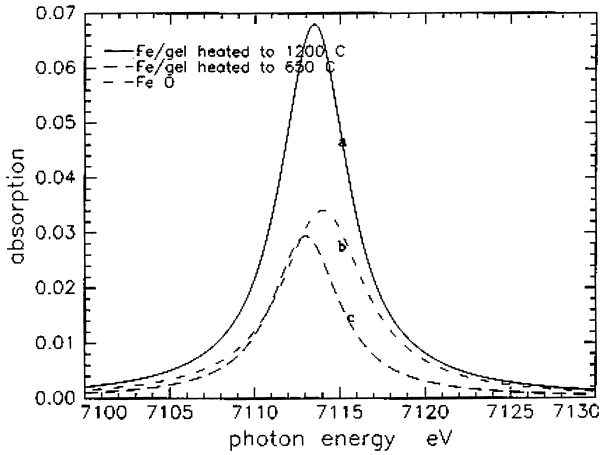

Figure 5. XANES spectra of the photoproduct in xerogel after photolysis (---), after heating to 650 °C (- - -), and after consolidation of the xerogel at 1200 °C (—).

intensity of an Fe_2O_3 standard, indicating that ≥99.9% of the iron present in the xerogel after photolysis is octahedrally coordinated Fe^{3+}. In contrast to the behavior in PVG, where consolidation occurs with a ≤12% change in the Fe^0/Fe^{3+} ratio, consolidating the xerogel at 1200 °C broadens the Mossbauer absorption and resolution of the absorption yields two doublets (Figure 4b). One exhibits an isomer shift of 0.40 ± 0.01 mm/s and a quadrupole splitting of 0.95 ± 0.01 mm/s, while the other exhibits an isomer shift of 0.23 ± 0.01 mm/s with a quadrupole splitting of 2.0 ± 0.01 mm/s. The XANES absorption shifts to 7114.5 eV and increases in intensity (Figure 5). Normalized to the intensity of the first EXAFS absorption of the consolidated sample, consolidation of the xerogel more than triples the intensity of the pre-edge feature at 7114.5 eV (Figure 5). Consolidation of the xerogel creates two forms of iron, and the relative intensities of the Mossbauer doublets indicate the two forms of iron are in a ratio of ca. 4/1 in the consolidated xerogel. The ratio of the two forms of iron is independent of the initial $Fe(CO)_5$ loading, 10^{-6} to 10^{-4} mol of $Fe(CO)_5$/g of the xerogel.

Consolidation of the photolyzed PVG samples does not lead to the changes evident during consolidation of the xerogel samples. EXAFS and XANES results show little change, and Mossbauer intensities show that consolidation occurs with a ≤12% change in the Fe^0/Fe^{3+} ratio.[19,20,31] However, consolidation of the PVG samples leads to photoproduct aggregation. In PVG, the particle size increases from ≤1 nm in diameter after photolysis to 3−4 nm in diameter in samples heated to 650 °C and 10 ± 1 nm in diameter in glasses consolidated at 1200 °C.[25] TEM analyses of the xerogel samples, on the other hand, fail to reveal any particles in xerogels after photolysis or in photolyzed samples heated to 650 °C and consolidated to a nonporous glass at 1200 °C. Regardless of the initial $Fe(CO)_5$ loading, the resolution of the TEM, ≥0.8 nm, implies that the photoproducts in the xerogel exist as either individual molecular species or aggregates ≤1 nm in diameter and remain ≤1 nm during consolidation and in the SiO_2 glass obtained by consolidation of the xerogel.

Discussion

PVG and base-catalyzed, dried TMOS/MeOH/H_2O xerogels are obtained by different processes and heated to different temperatures, but are structurally similar and possess chemically similar surface functionalities.[14b,15,17] Free and associated surface silanol groups populate both surfaces, and spectral subtraction suggests that the relative ratios of free to associated silanols are not that different in the two materials. A slightly broad absorbance at 3450 cm^{-1} in the xerogel indicates that, although dried under similar conditions, the xerogel contains slightly more chemisorbed water.

Both matrices are composed of 3−8 μm diameter silica nodules, which are themselves made up of smaller nodules ranging from 70 to 200 nm in diameter in the xerogel and from 100 to 600 nm in diameter in the PVG.[14b] Porosity derives from the space between the silica nodules, and N_2 adsorption−desorption yields an average pore diameter of 10 ± 1 nm for PVG, which agrees with a distribution of pore diameters with the majority in the 7 ± 2 nm diameter range.[14b,28] Both values suggest the smaller 70−200 nm aggregates, rather than the larger micrometer-sized aggregates, define the porosity in PVG as measured by N_2 adsorption−desorption. The TMOS/CH_3OH/H_2O xerogel is also nodular, but correlations between its porosity and structure are less apparent. The shape of the N_2 adsorption isotherm differs from that of PVG,[22,28] and the aggregates making up the xerogel, in general, are more irregular in shape than those in PVG. The sensitivity of calculated pore diameters to the structural details of the surrounding silica matrix[28] may account, in part, for the ranges of porosity, 0.5 nm to 1−2 μm, calculated from the N_2 adsorption−desorption isotherms in these TMOS/MeOH/H_2O xerogels.[14b,22]

The nodular composition of both materials creates the irregularity of their outermost surfaces, ±286 nm for the xerogel

and ±440 nm for PVG. The magnitude of the numbers suggests the irregularity measured by AFM is a composite of a number of different structural features. Neither material, however, exhibits a periodicity in its surface oscillations suggestive of a long-range, ≥5 μm, structural order. Both are indeed amorphous, porous materials characterized by a short-range order, implying their influence on an adsorbate, its chemistry, and its aggregation within the matrices arises from differences on length scales less than that evident in the topology of the two surfaces.

The striking structural difference is the topology of the individual SiO_2 nodules. The surfaces of the 100−600 nm diameter nodules in PVG are highly structured (Figure 1a) with 40 ± 20 nm high and 40 ± 20 nm wide "stalagmite-like" features. The uncertainty is large, but the dimensions of these features are within experimental error of the correlation length of PVG. Small-angle X-ray (SAXS) and neutron (SANS) scattering yields 22 ± 1 and 24 ± 1 nm, respectively, as the correlation length of PVG.[24,32] As the average length of uniform density, the correlation length indicates these stalagmite-like surface features (Figure 1a) are the smallest integral-structural units in PVG. Similar stalagmite-like features are also present on the surfaces of the 70−200 nm diameter SiO_2 nodules of the xerogel (Figure 1b), although the number present and their size are smaller than those found on PVG. The stalagmite-like features on the four xerogel samples examined (Figure 1b) range from 5 to 20 nm wide and from 10 to 20 nm high, with the majority falling in the range of 15 ± 5 nm wide and 15 ± 5 nm high. The correlation length of these specific xerogels has not been measured, but those reported for xerogels prepared in a similar manner are significantly smaller than the dimensions of the stalagmite-like features.[33] Woignier, Phalippou, and Vacher, for example, report the one-step base-catalyzed (5×10^{-2} N NH_4OH) hydrolysis of TMOS followed by high-temperature solvent extraction yields smooth uniform particles that assemble into larger fractal networks.[33a] Porod plots of the neutron scattering from the resulting xerogel yield a correlation length of <1.2 nm.[33a] Schaefer and Keefer prepared low-density, porous silicates by a one-step, base-catalyzed hydrolysis of fractally rough silicate precursors. The correlation lengths of these xerogels, 0.1−1.0 nm, suggest a bulk material composed of aggregates of smaller, uniform particles ≤1.0 nm in diameter.[33b−d] The data are limited, subject to a large uncertainty in the sizes of the structural features, and subject to structural variations arising from subtle differences in the preparative and drying procedures.[17] Nevertheless, the available correlation lengths, ≤1.0 nm, are significantly less than any of the structural features evident in the AFM images (Figure 1b). Unlike those on PVG, the stalagmite-like features on the xerogel surfaces are not integral units, but are themselves composites of smaller structural units. More important, these silica surfaces differ in the average length of structural uniformity or, conversely, the average distance between structural discontinuities. The differences in the photoproducts derived from $Fe(CO)_5$ and the subsequent formation of photoproduct nanoparticles in these amorphous matrices are attributed to differences in their correlation lengths.

The absence of elemental iron as a photoproduct in the dried TMOS/MeOH/H_2O xerogels differentiates the photochemistry of $Fe(CO)_5$ in the xerogel from that on PVG. Originally attributed to the larger amount of water in the xerogel,[20] its presence in one matrix and not the other, even though the amounts of water evolved from both matrices exceed the amount of $Fe(CO)_5$ adsorbed, and its lack of formation in xerogels dried at 200 °C for at least one month indicate that water content is not the sole determinant of photoproduct chemistry. The intensity of the XANES pre-edge feature establishes that the absence of Fe^0 in the xerogel is not simply a question of detection sensitivity. Normalized to the intensity of the first EXAFS absorption, the XANES intensity is within experimental error of that from an Fe_2O_3 standard, indicating that ≥99.9% of the iron photoproduct in the xerogel is octahedrally coordinated Fe(III). The absence of Fe^0 in the xerogel must arise from either differences in the primary photoprocesses of the $Fe(CO)_5$(ads) in the two matrices or differences in the chemistries of the primary photoproducts in the two matrices. The similarities of the absorption and DRIFT spectra of the adsorbed complex and the quantum efficiencies of the reaction suggest the difference is not due to differences in the primary photoprocesses.[21] Rather, the different product distributions arise from different chemistries of the primary photoproduct, an iron atom or a highly decarbonylated elemental iron species, in the two silica matrices.[21]

The Mossbauer absorption from the xerogel samples, a doublet with an isomer shift of 0.40 ± 0.01 mm/s and a quadrupole splitting of 0.95 ± 0.01 mm/s (Figure 4a), is not identical to that of the oxide formed in PVG, an isomer shift of 0.52 ± 0.05 mm/s with a quadrupole splitting of 0.64 ± 0.06 mm/s.[19,31] However, the isomer shifts are similar and both fall within the range reported for octahedrally coordinated Fe^{3+}.[34] The oscillations of the main EXAFS absorption are consistent with the Mossbauer data, yielding a central Fe(III) surrounded by 5.9 ± 1.0 oxygens at a distance of 1.8 ± 0.18 Å. The coordination number and the Fe−O bond length are within experimental error of the numbers, 5.9 ± 1.0 and 1.5 ± 0.15 Å, obtained for the oxide photoproduct formed in PVG, which is assigned to Fe_2O_3.[19,31] The Fe−O bond lengths of the oxides in both matrices are smaller than the Fe−O distances of ca. 2.0 Å in bulk iron oxides and closer to those in Fe_2SiO_4 formed in SiO_2 glasses.[20] In the absence of any indication of binding to either silica matrix (vide infra), the shorter bond lengths of these ≤1 nm diameter particles are attributed to distortions imposed by the surrounding silica matrix.

Incorporating Si into the first shell of the atoms surrounding a central iron in either matrix significantly degrades the fit, implying that Fe(III) does not form an Fe−Si bond in either matrix. More recent EXAFS spectra of the iron present in PVG yield similar results regarding the second shell of atoms about the central iron. At least in PVG, the EXAFS oscillations indicate the photochemically generated iron does not form Fe−Si or Fe−O−Si bonds, implying the particle does not formally bond to the PVG surface. The scattering intensities are not sufficient to identify the atoms present in the second

(32) Wiltzius, P.; Bates, F. S.; Dierker, S. B.; Wignall, G. D. *Phys. Rev. A* **1987**, *36* (6), 2991–4.

(33) (a) Woignier, T.; Phalippou, J.; Vacger, R. In *Better Ceramics Through Chemistry II*; Brinker, C. J., Clark, D. E., Ulrich, D. R., Eds.; Materials Research Society: Warrendale, PA, 1986; p 57. (b) Himmel, B.; Gerber, T.; Buerger, H. *J. Non-Cryst. Solids* **1987**, *91* (1), 122–36. (c) Brinker, C. J.; Keefer, K. D.; Schaefer, D. W.; Assink, R. A.; Kay, B. D.; Ashley, C. S. *J. Non-Crystal. Solids* **1984**, *63* (1−2)), 45–59. (d) Schaefer, D. W.; Keefer, K. D.; Brinker, C. J. *Polym. Prepr. (Am. Chem. Soc., Div. Polym. Chem.)* **1983**, *24* (2), 239–40.

(34) (a) Reis, S. T.; Mogus-Milankovic, A.; Licina, V.; Yang, J. B.; Karabulut, M.; Day, D. E.; Brow, R. K. *J. Non-Cryst. Solids* **2007**, *353* (2), 151–158. (b) Frischat, G. H.; Tomandl, G. *Glastech. Ber.* **1969**, *42* (5), 182–5. (c) Myson, B. O. *J. Non Cryst. Solids* **1987**, *95−96*, 247. Dyar, M. D. *Am. Mineral.* **1985**, *70*, 304.

shell of atoms about iron in the TMOS/MeOH/H_2O xerogels. Nonetheless, the structural and chemical similarities of the PVG and xerogel surfaces, the equivalence of the Fe−O bond lengths in both matrices, and the similarities of the Mossbauer spectra of the iron oxides in both matrices point to equivalent species in both matrices and an absence of chemical bonding to either matrix. This lack of bonding to the surface and the insensitivity of the Fe^0/Fe(III) ratio to air, adsorbed water, and even the water evolved at the elevated temperatures required for consolidation (1200 °C), which on a mole basis exceeds the number of moles of $Fe(CO)_5$ initially present in the PVG samples, also suggest the photoproducts are not individual species, but small aggregates. Taken collectively with the differences in particle growth in the two matrices (vide infra), the data suggest the chemistry of the primary photoproduct, and ultimately the photoproducts observed, is dictated by the relative rates of aggregation and oxidation in the two matrices. Provided the rate of aggregation exceeds the rate of oxidation, aggregation occurs and oxidation is limited to the outermost Fe atoms of the aggregates. Linderoth, Morup, and Bentzon, for example, report that 5 nm diameter iron particles generated in air react immediately to form a 1−2 nm thick oxide coating which curtails further oxidation of the elemental iron core.[35] The photoproducts initially detected in PVG are ≤1 nm in diameter. Nonetheless, they appear to be sufficient to curtail further oxidation of the elemental iron core of the particle, since the Fe^0/Fe(III) ratio changes by ≤12% on standing in air, during subsequent particle growth at higher temperatures, or during consolidation of the PVG at 1200 °C. The absence of Fe^0 oxidation during consolidation is particularly intriguing since the amount of water evolved, on a mole basis, is 27−29 times the amount of $Fe(CO)_5$ originally adsorbed onto the PVG samples.

The absence of Fe^0 in the xerogel is attributed to less extensive aggregation, which is somewhat surprising since the xerogel surface is smoother (Figure 1b) than that of PVG (Figure 1a). However, the correlation length, ≤1 nm in the xerogel,[33] as opposed to 23 ± 1 nm in PVG,[24,32] defines the average length of uniform density or, conversely, the average spacing between discontinuities in the structures of these amorphous silicas. A spacing of Fe^0−Fe_2O_3 particles in consolidated PVG equivalent to its correlation length, 22 ± 1 nm, suggests these structural discontinuities are the sites at which aggregation of the decarbonylated iron photoproduct initiates. $Fe(CO)_5$ diffusion during photolysis increases the amount of iron in the outermost volumes of PVG by ca. 30%, which corresponds to ca. 1 $Fe(CO)_5$ molecule/nm^2. In the absence of any indication of bonding to the silica surface, the photoproducts are assumed to be free to move a distance defined by the uniformity of the surface, or its correlation length. Assuming only the photoproducts generated within a circular area defined by a radius equal to half the correlation length are capable of aggregating, a surface coverage of 1 $Fe(CO)_5$/nm^2 and a PVG correlation length of 22 ± 1 nm places 432 Fe photoproducts within an aggregation distance in PVG, whereas ≤1 Fe photoproduct lies within the correlation length of the xerogel, ≤1 nm. Assuming similar levels of aggregation must be achieved in both matrices to prevent complete oxidation since both matrices possess similar hydroxylated surfaces with only slightly more chemisorbed water in the xerogel, the shorter correlation length of the xerogel, ≤1 nm, favors the formation of a larger number of smaller particles, none of which achieve sufficient aggregation to prevent complete oxidation. The longer correlation length of PVG, on the other hand, favors a more extensive, perhaps more rapid, aggregation and a particle size sufficient to prevent complete iron oxidation. Assuming spherical particles consisting of an Fe^0 core surrounded by α-Fe_2O_3 cladding with equal numbers of iron atoms in the core and cladding since the Mossbauer intensities correspond to 42 ± 12% Fe^0,[19,31] the densities of the bulk materials indicate a spherical particle containing 432 atoms distributed among the core and cladding has a diameter of ca. 3.0 nm.[14b] Since 3−4 nm diameter Fe^0−Fe_2O_3 particles are detectable in PVG,[39] the absence of particles ≥1 nm in diameter after photolysis suggests that the actual aggregation that occurs in PVG at room temperature is less. Nonetheless, it is sufficient to limit oxidation to the outer periphery of the aggregate, thereby leading to a core−shell nanoparticle. More recent, detailed analyses of the TEM images of the 3−4 nm diameter particles formed in PVG heated to 650 °C are indeed consistent with the formation of core−shell nanoparticles.[37] The data suggest that these iron photoproducts do not bond to either silica matrix. Even if bonding occurs at the discontinuities in the matrix, however, the result is the same; the correlation length of these silica matrices, as opposed to the topology of their surfaces (Figure 1), or their water content, determines the chemistry of the iron photoproducts generated in these amorphous silica matrices and, in turn, the structure of the nanoparticles formed. Shorter correlation lengths curtail aggregation, thereby favoring complete photoproduct oxidation, whereas a longer correlation length favors aggregation, thereby limiting oxidation to the outer periphery and formation of a core−shell nanoparticle with the reduced and oxidized metal distributed between the core and cladding, respectively. Particle growth in the two matrices provides further evidence of fundamental differences in photoproduct diffusion and aggregation.

$Fe(CO)_5$ diffusion during photolysis dramatically increases the amount of iron in the outermost volumes of PVG, but photolysis per se fails to lead to aggregation and particle growth.[25] Particles ≤ 1 nm in diameter imply diffusion of the iron photoproducts is limited at room temperature. Particle growth occurs only in PVG and only during subsequent heating, with the Fe^0−Fe_2O_3 particle diameter increasing from ≤1 nm after photolysis to 3−4 nm in samples heated to 650 °C and 10 ± 1 nm in samples consolidated at 1200 °C. The particle diameter in consolidated PVG is within experimental error of the initial pore diameter, 9 ± 2 nm,[14b,28] and the average interparticle spacing, 22 ± 1 nm, is within experimental error of its correlation length.[24,32] The correspondence between particle diameter and interparticle spacing and the structural characteristics of the porous glass implies the porous glass acts as a template for particle growth. Therefore, particle growth must occur prior to contraction and collapse of the pore structure, which begins around 600 °C (Figure 2). Otherwise, consolidation of the matrix, which reduces the sample volume by 30−35%,[14b,18] is expected to produce ranges of particle diameters and interparticle spacings. As noted above, the photoproduct in PVG appears to be a ≤1 nm diameter aggregate composed of an Fe^0 core surrounded by Fe_2O_3. The insensitivity of the Fe^0/Fe(III) ratio to air and water evolved during subsequent heating and consolidation implies particle growth occurs with minimal disruption of the Fe_2O_3 cladding surrounding the Fe^0 core. As

(35) (a) Linderoth, S.; Moerup, S.; Bentzon, M. D. *J. Mater. Sci.* **1995**, *30* (12), 3142–8. (b) Linderoth, S.; Bentzon, M. D.; Moerup, S. *Nucl. Instrum. Methods Phys. Res., B* **1993**, *B76* (1−4), 173–4.

(36) Reference 17, Chapter 9.

(37) Armasinghe, D. A. Microstructural Environments and Redox States of Iron in Random and Ordered Porous Silica Matrices. Ph.D. Thesis, City University of New York, 2008.

Scheme 1

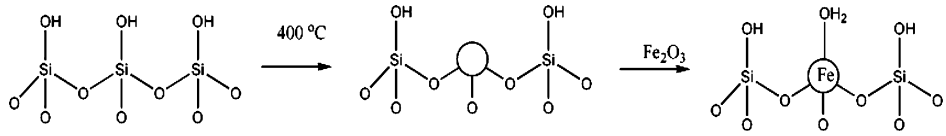

the temperature increases, the smaller $Fe^0-Fe_2O_3$ aggregates formed after photolysis diffuse across the silica surface and collect within the pores of PVG. A first approximation of the diffusion distance then is the average distance between the pores. The PVG samples used in these experiments are 25 mm × 25 mm × 2 mm, and consolidation reduces their volume by 30−35%, or an average of 4.1×10^{-7} m^3. Taking the reduction in volume on consolidation as the total pore volume within the sample, and 5 nm as the average pore radius,[18,28] there are ca. 8.5×10^{17} pores in the sample. Assuming these are randomly distributed throughout the 1.3×10^{-6} m^3 volume of the sample, the average volume between the pores is $(1.3 \times 10^{-6}\ m^3)/(8.5 \times 10^{17})$ or 1.5×10^{-24} m^3. The average distance between the pores depends on the shape of this volume and ranges from 1 nm if spherical to 11 nm if cubic. The calculation is an approximation, but it yields distances on the order of the correlation length of the glass and the average spacing between the $Fe^0-Fe_2O_3$ particles in the consolidated glass, 22 ± 1 nm, suggesting that the average diffusion length necessary for particle growth within the PVG matrix is indeed on the order of the correlation length of the glass.

While the particle size increases in PVG, equivalent growth does not occur during consolidation of the xerogel samples. TEM fails to detect particles after photolysis or after consolidation of the xerogel at 1200 °C, implying the photoproduct remains ≤1 nm in diameter after photolysis and in the consolidated xerogel. With both matrices consolidated at 1200 °C, attributing the differences in particle growth in these matrices to differences in the bonding to the surfaces seems unlikely. In fact, barrier(s) to particle growth exist in both matrices since aggregation and particle growth in PVG occur only during subsequent heating.[25] With PVG serving as a template, particle growth must occur prior to collapse of the pore structure (Figure 2), or at ≤600 °C. With similar oxides (the outer surface of the elemental iron in PVG is coated with an oxide) dispersed on chemically similar silica surfaces, attributing the differences in particle growth to different activation barriers arising from different bonds to the silica surface seems unlikely. It is also unlikely to attribute differences in particle size to the surface morphology or topology since the particle size increases on the more structured PVG surface, but not on the smoother xerogel surface (Figure 1).

Instead, differences in particle growth during thermal consolidation of these silica matrices are attributed to the changes the silica matrices undergo during heating and consolidation. No measurable change in surface area occurs on heating PVG to 600 °C, at which point the surface area declines smoothly (Figure 2) as the matrix consolidates to a nonporous glass. Heating the xerogel, on the other hand, leads to a region between 300 and 500 °C in which the surface area oscillates both increases and decreases (Figure 2). Each TMOS/MeOH/H_2O xerogel exhibits oscillations in surface area in the 300−500 °C range, and each exhibits two exothermic processes at 380 and 440 °C. The 380 °C process is due to the decomposition of $Si-OCH_3$ functionalities in the xerogel, and the appearance of a light gray coloration suggests some decomposition to elemental carbon. The 440 °C process occurs with a loss of the gray coloration and is due to desorption of the carbonaceous decomposition products. Although porous, desorption of the gaseous decomposition products is a violent process in which some of the desorbing gases actually explode from the consolidating silica, forming sharp-edged craters on the xerogel surfaces (Figure 3). In view of the sensitivity of the surface area and pore diameter calculated from gas adsorption−desorption data to the structural details of the adsorbent,[28] the oscillations in surface area are attributed to changes in the silica matrix as a result of violent desorption of the gaseous decomposition products. Desorption creates a dynamic surface which in turn affects diffusion and aggregation. Devoid of organic precursors, equivalent desorption processes do not occur in PVG (Figure 2). This porous silica consolidates smoothly and, without the disruptive effects of gaseous byproduct desorption, provides a surface on which aggregation and particle growth occur. Assuming diffusion and aggregation initiate at similar temperatures in the two matrices since similar iron oxides diffuse on chemically similar silanol surfaces, and these temperatures, which must be ≤600 °C, overlap the 300−500 °C range, the difference in iron oxide particle growth is attributed to the disruptive effect of the desorption of the gaseous byproducts from the xerogels.

Consolidation of PVG leads to particle growth with a ≤12% change in the Fe^0/Fe(III) ratio,[25] while consolidation of the xerogel fails to increase the particle size, but chemically changes some of the initially present octahedrally coordinated Fe(III). Resolution of the Mossbauer absorption yields two doublets (Figure 4b). The doublet with an isomer shift of 0.40 ± 0.01 mm/s and a quadrupole splitting of 0.95 ± 0.01 mm/s is equivalent to that observed after photolysis, and the values fall within the ranges reported for Fe_2O_3. The other exhibits an isomer shift of 0.23 ± 0.01 mm/s with a quadrupole splitting of 2.0 ± 0.01 mm/s and is consistent with tetrahedrally coordinated Fe(III). EXAFS and XANES corroborate the change in coordination. The XANES absorption shifts to 7114.5 eV and, normalized to the intensity of the first EXAFS absorption of the consolidated sample, more than triples the intensity of the pre-edge feature at 7114.5 eV (Figure 5). Resolution of the oscillations on the main EXAFS absorption places 3.9 ± 1.0 oxygens at a distance of 1.8 ± 0.18 Å about the central iron. The relative intensities of the Mossbauer doublets are in a ratio of ca. 4/1, indicating that ca. 20% of the initially present octahedrally coordinated Fe(III) converts to tetrahedral coordination on consolidation of the xerogel. The appearance of tetrahedral Fe(III) in the xerogel is also attributed to the desorption of the gaseous byproducts since there is no evidence of tetrahedral Fe(III) in PVG, and an increase in the intensity of the XANES spectrum is first evident in samples heated to 650 °C (Figure 5). The explosive-like release of the gaseous byproducts through the consolidating surface (Figure 3) is thought to break Si−O bonds in the silica matrix as the gas escapes. Since there is no evidence of Si in the first shell of atoms about the tetrahedral iron, desorption is thought to create a Si vacancy in the xerogel matrix that becomes occupied by

Fe(III), Scheme 1. Replacing Si with Fe(III), however, creates a charge−size imbalance. In these SiO_2 matrices, Si is formally 4+ with a diameter of 0.026 nm, whereas Fe is formally 3+ with a diameter of 0.050 nm. The size imbalance suggests that Fe(III) is not incorporated into the bulk SiO_4 matrix, but is limited to the outer surfaces of the matrix, which may account for the small fraction, 23 ± 3%, of iron that converts from O_h to T_d coordination. The charge imbalance requires either a counterion or a structural anomaly, either of which could affect the spectroscopic properties of the doped glasses. Since the surfaces of these porous silicas contain $HO-Si(O-Si)_3$, a possible structure that is formally electrically neutral, thereby satisfying the charge imbalance, is $H_2O-Fe(O-Si)_3$, where water coordinates to an Fe(III) occupying a silica surface site.

Conclusion

The distribution of Fe^0 and Fe_2O_3 photoproducts derived from the 488-nm photolysis of $Fe(CO)_5$ physisorbed onto PVG and dried TMOS/MeOH/H_2O xerogels reflects a competition between aggregation and oxidation. Sufficient aggregation occurs in PVG to limit oxidation to the outer periphery, thereby producing a core−shell nanoparticle consisting of an Fe^0 core surrounded by an Fe_2O_3 cladding, whereas in the xerogel aggregation is limited and Fe_2O_3 is the sole reaction product. The differences in the extents of aggregation are a consequence of the correlation lengths of the two silica matrices as opposed to the topology of their surfaces. Although the photoproducts are not bound to the silica surface, thermal energy is required for particle growth. The longer correlation length of PVG, 22 ± 1 nm, favors the formation of a smaller number of larger $Fe^0-Fe_2O_3$ particles with the glass matrix acting as a template defining both the particle diameter, 10 ± 1 nm, and the interparticle spacing, 22 ± 1 nm. The shorter correlation length of the xerogel, ≤1 nm, favors the formation of a larger number of smaller particles. Decomposition of the xerogel precursors creates a dynamic surface that further curtails aggregation, thereby limiting the particle size to ≤1 nm in diameter in the consolidated xerogel. Desorption of the decomposition products fractures some of the developing silica framework, creating Si deficiencies populated by iron to form a mixture of octahedrally coordinated Fe(III) in the form of Fe_2O_3 and tetrahedrally coordinated Fe(III) in the form of $H_2O-Fe(O-Si)_3$ on the xerogel surfaces.

Acknowledgment. Support of this research by the National Science Foundation (Grants CHE-0514458 and CHE-0079040), the Air Force Office of Scientific Research, the donors of the Petroleum Research Fund, administered by the American Chemical Society, and the City University of New York Center of Advanced Technology in Photonics, funded by the New York State Science and Technology Foundation, is gratefully acknowledged. We thank Corning Inc. for samples of porous Vycor glass.

JA9031874